Cellular and Molecular Biology

Journal homepage: www.cellmolbiol.org

Evaluation of Tumor Resection Effect of Color Doppler Ultrasound Positioning Guided Breast-Conserving Surgery Using Nano-Contrast Agent

Yun Fang[1], Wei Lin[2*], Yuwang Zhou[1], Wenwu Wang[2], Xueping Liu[1]

[1]Ultrasonography Department, The Quzhou Affiliated Hospital of Wenzhou Medical University, Quzhou People's Hospital, Quzhou, 324000, China

[2]Department of Breast and Thyroid Surgery, The Quzhou Affiliated Hospital of Wenzhou Medical University, Quzhou People's Hospital, Quzhou, 324000, China

ARTICLE INFO

Original paper

Article history:
Received: November 04, 2021
Accepted: March 14, 2022
Published: March 31, 2022

Keywords:
Fe_3O_4, nano-contrast agent, magnetic lipid ultrasound microbubbles, color doppler ultrasound positioning guidance, breast-conserving surgery, tumor resection

ABSTRACT

This study aimed to explore the clinical value of Fe_3O_4-based magnetic lipid nano-contrast agent in breast-conserving surgery for breast cancer using color doppler ultrasound positioning and to analyze the tumor resection effect of breast-conserving surgery. On account of Fe_3O_4 magnetic nanoparticles prepared by the chemical co-precipitation method, magnetic lipid ultrasonic microbubbles (MLU-MBs) were prepared by mechanical oscillation method after surface modification using polyethylene terephthalate (PET). Characterization and analysis of the prepared MLU-MBs were performed using scanning electron microscopy (SEM), energy spectrometer, transmission electron microscopy (TEM), and Fourier infrared spectroscopy (FIRS). A high-frequency alternating magnetic field was used to detect the heating of MLU-MBs and the color ultrasound machine was applied to observe the enhancement effect of the MLU-MBs on rabbit liver images. 92 patients undergoing breast-conserving surgery for breast cancer were taken as the research objects and were divided into a nano group (MLU-MB as contrast agent) and a control group (conventional contrast agent) according to the differences of intraoperative contrast agents, with 46 cases in each group. Before the surgery, both groups of patients were positioned and marked the tumor boundary under ultrasound. The differences in tumor volume (TV), amount of tissue removed, resection rate, and positive rate (PR) of resection margins were compared between the two groups. The results showed that the Fe_3O_4 magnetic nanoparticles were particles with an average particle size of about 15nm, and their iron and oxygen percentages were consistent with the content of Fe_3O_4. The MLU-MBs were spherical particles of about 1120nm, containing phosphorus (P), oxygen(O), and Ferrum (Fe). Under 30A and 220kHz of output current and frequency, the temperature rise of the MLU-MBs suspension with different concentrations was 10 ~ 60°C, and the temperature was constant after heating for 45 minutes. Compared with the rabbit liver parenchyma, the image was greatly enhanced. TV, the amount of tissue removed, the resection rate, and the PR of resection margins in the nano group were obviously lower than those in the control group (P<0.05). It showed that MLU-MBs with good image enhancement effect on account of Fe_3O_4 magnetic nanoparticles were successfully prepared and it could effectively reduce the PR of normal tissues and the positive margin of two-fold resection during breast-conserving surgery for breast cancer and showed good accuracy and stability.

DOI: http://dx.doi.org/10.14715/cmb/2022.68.3.40

Introduction

Breast cancer is one of the most common malignant tumors in women. In recent years, the incidence of breast cancer has been on the rise and it is getting younger (1). The proportion of new cases and death cases rank first in cancer (2). Light trauma, fast postoperative recovery, and good post-cosmetic effect are the advantages of breast-conserving surgery (3), with a low recurrence rate after breast-conserving surgery, and has become the best surgical method for the treatment of early breast cancer (4). Currently, breast cancer tumor localization methods are mainly preoperative ultrasound localization, guidewire localization, radiation-guided localization of hidden lesions, tracer guidance, radioactive particle localization, intraoperative ultrasound localization, palpation-guided, and so on (5). Guidewire puncture milk labeling and positioning method can reduce the difficulty of surgery and improve the removal rate of lesions and pathological diagnosis rate, but it is expensive (6). Palpation-guided breast-conserving surgery has low positioning accuracy and is prone to

*Corresponding author. E-mail: qzlw19771022@126.com

excessive volume of excised tissue and positive incision margin (7). Ultrasound-guided preoperative guidewire positioning is considered to be the gold standard for breast cancer patient positioning, which can be used to determine the size and location of lesions by ultrasound images to improve surgical efficiency (8).

Although there are significant advantages of disease diagnosis in ultrasound, there are still poor echo signals and imaging effects in the detection of obese people, which are prone to misdiagnosis(9), and the accuracy of soft tissue diagnosis needs to be further improved (10). Injecting an ultrasonic contrast agent (UCA) into the human body can significantly improve the ultrasonic return signal and increase the sensitivity and accuracy of ultrasonic imaging (11). UCA is mainly composed of hollow microbubbles less than 8μm in diameter filled with air or inert gas. Microbubbles enter blood vessels through intravenous injection, reflect and scatter acoustic signals by virtue of their hollow properties so as to enhance tissue echo signals and improve ultrasound imaging quality (12). At present, there are many reports about ultrasonic contrast agents, mainly lipids, proteins, surfactants, and polymers. Among them, lipid and protein ultrasonic contrast agents collapse and rupture when blood pressure is high due to the low molecular weight of air (13). Magnetic lipid ultrasonic microbubbles (MLU-MBs) contrast agent is formed by wrapping inert gas with lipid, which has good stability in blood and a long time in vivo, but its size is difficult to control and its attenuation in vivo is difficult to predict (14).

In summary, ultrasonic nanocontrast agents should be further optimized in clinical use. In this study, on account of the advantages of Fe_3O_4 nanoparticles, a new MLU-MBs was prepared by surface modification of Fe_3O_4 nanoparticles and used in the breast-conserving treatment guided by color ultrasound localization to explore its value in breast-conserving tumor resection, so as to provide a reference basis for clinical breast-conserving tumor resection guided by color ultrasound localization.

Materials and Methods

Preparation of Fe_3O_4 nanoparticles

Fe_3O_4 nanoparticles were prepared by an improved chemical coprecipitation method. The specific operation method was as followings: It was advised to take a certain amount of $FeCl_3$-$6H_2O$ (Shanghai Chaoyan Biotechnology Co., LTD.) and $FeCl_2$-$4H_2O$ (Beijing Kangpuhuiwei Technology Co., LTD.), configure 0.1mol/L Fe^{3+} and Fe^{2+} solutions, respectively. Fe^{3+} and Fe^{2+} solutions were mixed at a volume ratio of 5:3. Under the protection of N_2, 1.5mol/L NHOH was added while stirring until the pH of the reaction solution was 9. The precipitates in the solution turned black. It was suggested to rinse the black precipitate with deionized water 3 to 5 times until the solution pH was 7 and to dry the precipitate in a vacuum for later use.

Preparation of MLU-MBs

Fe_3O_4 nanoparticles were dissolved in 4.5g/L oxalic acid solution and the supernatant was centrifuged at 8000rpm after 30min of ultrasound. The precipitation was suspended in phosphate buffer, and polyethyleneimine (PEI) was mixed with an appropriate amount during the ultrasonic process for 1.5h to fully form stable PEI/Fe_3O_4 nanoparticles. After repeated washing with distilled water, PEI/Fe_3O_4 nanoparticles were obtained after drying. Distearoylphosphatidlycholine (DSPC), diphenylphosphinoethane (DPPE), and diphenyl phosphoryl azide (DPPA) were added to the flask in a ratio of 1:1:1 and mixed well, denoted as solution 1. At the same time, organic solvent 2 was mixed with chloroform and isopropanol in a ratio of 2:1. The above solution 1 was dissolved in organic solvent 2, treated with ultrasound for 20min and heated at 85°C for 30min. The mixed solution of glucose and propylene glycol (glucose: propylene glycol = 4:1) was added. After 30min of ultrasound, 40mg of polyethylene glycol 4000 (PEG 4000) was added and heated at 60°C for 30min to produce lipid suspension. A certain amount of PEI/Fe_3O_4 and gelatin was added to the lipid suspension, stirred and mixed, 100μL tangu80 was added, stirred for 10min, 1mL sulfur hexafluoride (SF6) gas was filled with a 5mL syringe, and MLU-MBs was obtained by oscillating for 60 seconds in a 4500Hz mechanical oscillator. The specific preparation process of MLU-MBs is shown in Figure 1.

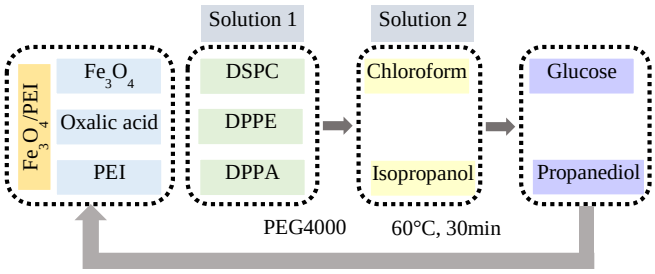

Figure 1. Preparation of MLU-MBs.

Characterization analysis of MLU-MBs

A certain amount of magnetic Fe_3O_4 nanoparticles and MLU-MBs were dissolved in anhydrous ethanol for 15min. A pipette gun was carefully added to the copper wire to prepare electron microscope samples. The morphology of magnetic Fe_3O_4 nanoparticles and MLU-MBs were observed under a scanning electron microscope (SEM) (Hitachi, Japan) and scanning electron microscope energy spectrometer (FEI, USA). Transmission electron microscopy (TEM), Fourier transform infrared spectroscopy (FTIR), energy dispersive spectrometer (EDS), and particle size measuring instrument were used to characterize and analyze MLU-MBs, and the temperature rise of magnetic lipid microbubbles (MLMs) was detected under high frequency alternating magnetic field (AMF).

In vivo ultrasound imaging of MLU-MBs

New Zealand white rabbits aged from 24 to 28 weeks were anesthetised by intravenous injection of 3% pentobarbital sodium. After the anesthesia was successful, the abdominal hair removal and abdominal ultrasound imaging were performed, and the initial imaging was recorded. Then, a certain amount of MLMs was injected into the ear veins of rabbits. After 5 seconds, the liver images of rabbits were observed and recorded under real-time dynamic ultrasound imaging.

Subjects and groups included

92 breast cancer patients who received breast-conserving surgery in the Hospital of Wenzhou Medical University from January 2019 to January 2021 were selected as the research subjects, and the age distribution of the patients ranged from 25 to 83 years old, with an average age of 45.51±9.76 years old. Tumor staging: 81 cases of T1 stage, 8 cases of T2 stage, and 3 cases of T31 stage. Tumor size distribution range: 7nm~49nm. The mean tumor size was 27.75 ± 6.47nm. The distribution of different molecular subtypes of breast cancer patients was as followings: There were 37 cases of Luminal A type, 25 cases of Luminal B type, 19 cases of Her2 overexpression type, and 11 cases of triple-negative type. The distribution of postoperative pathological types was as followings: There were 69 cases of invasive ductal carcinoma, 18 cases of intraductal carcinoma, 2 cases of mucinous carcinoma, 1 case of chemoplastic carcinoma, 1 case of invasive lobular carcinoma, and 1 case of mixed carcinoma. According to different intraoperative contrast agents, patients were divided into a nano group (MLU-MB as contrast agent) and a control group (conventional contrast agent), with 46 cases in each group. There were two requirements in the inclusion criteria. First, people were confirmed to be breast cancer patients by preoperative needle biopsy. Second, there were no lumps in the remaining quadrants of the breast. There were five requirements in the exclusion criteria. First, patients had ipsilateral multicentric lesions. Second, patients had a history of breast surgery and radiotherapy. Third, the lesions present in patients had microcalcification without mass. Fourth, patients received neoadjuvant chemotherapy. Fifth, people were pregnancy or lactation patients. The experimental procedure of this study was approved by the ethics committee of the Hospital of Wenzhou Medical University and all the subjects included in the study were signed informed consent.

Ultrasonic examination methods

Color doppler ultrasound (Philips) probe was used to mark tumor boundary on skin surface before and during breast-conserving surgery. The patient was placed in a supine or lateral decubitus position, and the tumor boundary was marked with a color ultrasound probe at 10-12Hz, and the ideal resection range (within 1cm around the tumor boundary) was marked. After the patient was anesthetized, the skin tissue was cut open and the resection was guided in real-time by 10Hz ultrasonic probe. The tumor boundary and ideal resection boundary were marked by multiple layers and multiple points. The tumor was removed, the direction and the position of the resection margin were marked.

In the control group, SonoVue microbubble suspension (Bracol, Italy) was extracted with a 1mL syringe during ultrasound examination and MLMs prepared by the same volume were injected into the nano group. 0.5mL was subcutaneously injected into the 5mm edge of the mass and observed for more than 5 minutes after the contrast agent was injected.

Observation indicators

The length, width, height of the tumor, and the excised tissue were measured and recorded. The specific algorithms for tumor volume (TV), ideal tumor volume (iTV), and actual tumor volume (aTV) were as follows:

$$TV = \frac{4}{3\pi\left(L_1/2 \times W_1/2 \times H_1/2\right)}$$

$$iTV = \frac{4}{3\pi\left[L_1/(2+1) \times W_1/(2+1) \times H_1/(2+1)\right]}$$

$$aTV = \frac{4}{3\pi\left(L_2/2 \times W_2/2 \times H_2/2\right)}$$

In the above equations, L_1, W_1, and H_1 represented the tumor length, width and height, respectively. L_2, W_2, and H_2 represented the length, width, and height of the actual resected tissue, respectively. The differences between TV excised TV, excision rate, and positive margin were compared between the two groups.

Statistical methods

SPSS19.0 statistical software was used for data processing. The mean ± standard deviation of measurement data was expressed as ($\bar{x} \pm s$). The statistical data was expressed as percentage % and χ^2 test was used, $P<0.05$ indicated that the differences were statistically significant.

Results and discussion

Characterization of magnetic Fe_3O_4 nanoparticles and MLU-MBs

In this study, magnetic Fe_3O_4 nanoparticles prepared by the chemical coprecipitation method were black powder, and fine particles were observed under SEM. They were scattered or aggregated into sheets with an average particle size of about 15nm (Figure 2A). Under the light, MLU-MBscould was round and had an obvious lipid membrane in the outer layer, with good dispersion (Figure 2B). Under SEM, it was approximately spherical with good dispersion, and its average particle size was about 1120nm (Figure 2C). This particle size could ensure that the microbubbles pass through the pulmonary circulation without causing embolism (15).

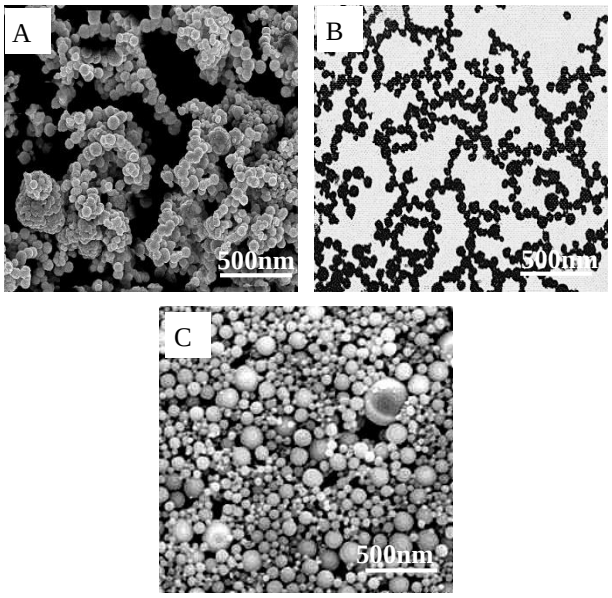

Figure 2. SEM and light microscope of nanoparticles. (Figure A: Fe_3O_4 magnetic nanoparticles SEM. Figure B: Light microscopy of MLU-MBs. Figure C~E: SEM images of MLU-MBs.)

EDS was used to analyze the composition of Fe_3O_4 magnetic nanoparticles (Figure 3). Iron and oxygen were contained in Fe_3O_4 magnetic nanoparticles. Iron accounted for 72.03% and oxygen accounted for 27.97%. The mass percentage of iron and oxygen was consistent with the mass percentage of iron and oxygen in Fe_3O_4 (16).

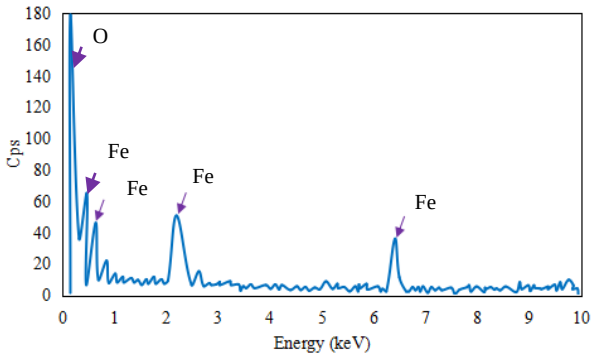

Figure 3. Energy spectrum of Fe_3O_4 magnetic nanoparticles.

Analysis of MLU-MBs (Figure4) showed that MLU-MBs mainly contained three elements,

phosphorus, oxygen, and iron. Iron and oxygen were magnetic materials with phospholipid composition, indicating that MLMs were successfully prepared.

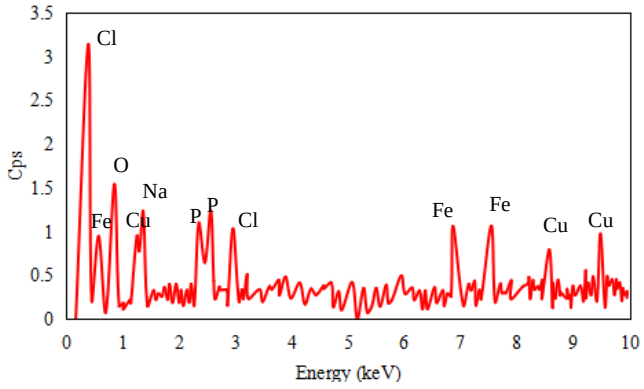

Figure 4. MLU-MBs.

FIRT results of MLU-MBs

IR results of magnetic Fe_3O_4 nanoparticles and MLU-MBs were analyzed (Figure 5). Compared with Fe_3O_4 magnetic nanoparticles, PEI-modified MLU-MBs showed three -CH_2 shear vibration characteristic waves at 1695cm^{-1}, 1495cm^{-1}, and 1585cm^{-1}. At 2905cm^{-1} and 3115cm^{-1},-NH_2 asymmetrical and symmetrical stretching vibration characteristic peaks of PEI appeared, respectively. This indicated that there were -NH_2 and -CH_2 characteristic peaks on the surface of MLU-MBs, and PEI was adsorbed on the surface of Fe_3O_4 magnetic nanoparticles (17).

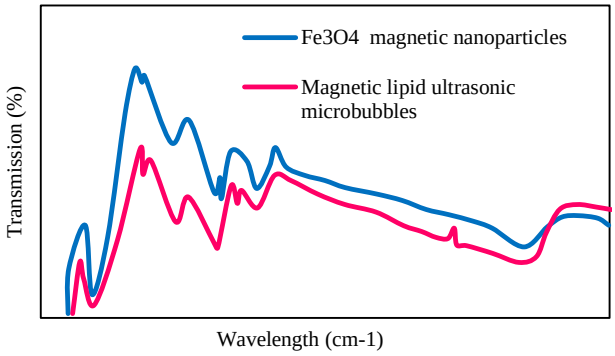

Figure 5. IR spectra of magnetic Fe_3O_4 nanoparticles and MLU-MBs.

Magnetic induction heating characteristics of Fe_3O_4 magnetic nanoparticles and MLU-MBs

The magnetic induction heating characteristics of Fe_3O_4 magnetic nanoparticles were analyzed (Figure 6). As the concentration increased, the temperature of Fe_3O_4 magnetic nanoparticles increased significantly. At the same concentration, the temperature of Fe_3O_4 magnetic nanoparticles increased first and stabilized with the extension of heating time. The temperature range of Fe_3O_4 magnetic nanoparticle suspended with different concentrations was 30~60°C, and the temperature remained constant after heating for 20min.

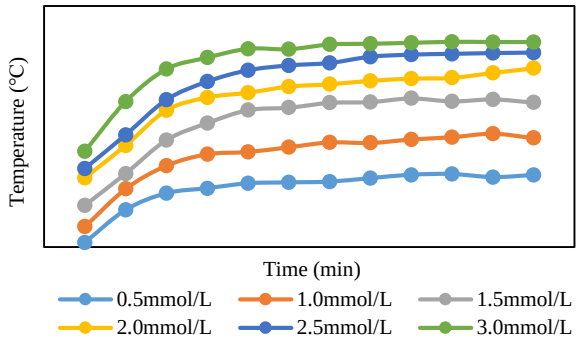

Figure 6. Magnetic induction heating diagram of Fe_3O_4 magnetic nanoparticles.

The magnetic induction heating characteristics of MLU-MBs were analyzed (Figure 7). The temperature rise range of MLU-MBs suspension with different concentrations was 10-40°C, and the temperature remained constant after heating 15min. When the magnetic field intensity was constant, the heating capacity of magnetic materials was significantly positively correlated with its concentration under the action of the magnetic field (18).

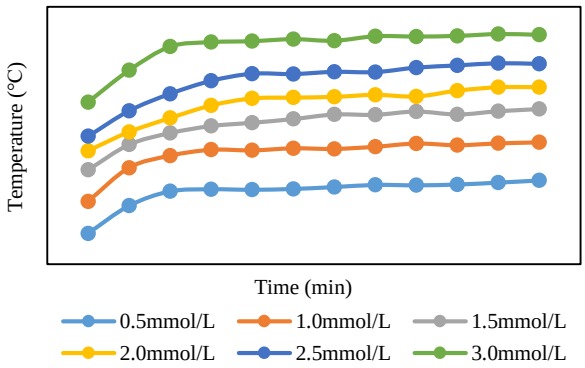

Figure 7. Magnetic induction heating of MLU-MBs.

In vivo ultrasound imaging of MLU-MBs in animals

Real-time ultrasonic imaging was performed on the livers of the white rabbits and the results were analyzed. Before the injection of the contrast agent,

tissues and organs in the liver of the white rabbits could not be distinguished and no echo signal could be detected (Figure 8A). After MLU-MBs were injected at the ear edges of the white rabbits, contrast agent filling was observed in the liver vessels and enhanced echo in the liver parenchyma (Figure 8B). The results indicated that MLU-MBs had better enhancement effect on ultrasonic development in vivo. As the shell membrane of microbubbles, the acoustic response of the lipids was good and the microbubbles were easy to generate echoes (19).

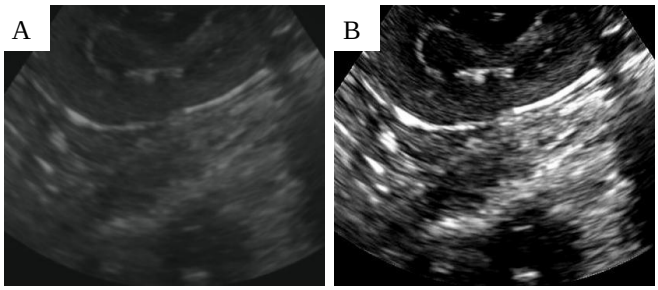

Figure 8. Ultrasound images of liver parenchyma in rabbits. (Figure A: Before the injection of MLU-MBs. Figure B: After the injection of MLU-MBs.)

Comparison of basic data between the two groups

The age, body mass index (BMI), the proportion of patients at different tumor sites, and the proportion of patients at different tumor stages of the two groups were compared and analyzed (Table 1). There were no significant differences in age, BMI, the proportion of patients at different tumor sites, and the proportion of patients at different tumor stages between 2 groups (P>0.05).

Table 1. Comparison ofbasic data between the two groups.

Groups	Control group (n=62)	Nano group (n=33)	T value or χ^2 value	P value
Age (years old)	51.17±8.12	53.12±7.87	1.859	0.275
BMI (kg/m^2)	24.41±2.58	23.87±3.51	2.319	0.181
Tumor location			6.255	0.147
Outer upper quadrant [cases, (%)]	22 (47.83)	23 (50.00)		
Other quadrants [cases, (%)]	24 (52.17)	23 (50.00)		
Tumor staging			7.128	0.188
T1[cases, (%)]	41 (89.13)	40 (86.96)		
T2[cases, (%)]	4 (8.70)	4 (8.70)		
T3[cases, (%)]	1 (2.17)	2 (4.35)		

TV was compared between the two groups

TV, iTV, aTV, and cardiac reverse remodeling (CRR) were compared between the two groups (Figure 9). TV, iTV, aTV, and CRR were 1.47±0.86cm^3, 18.96±1.83cm^3, 19.54±1.99cm^3, and 0.87±0.09cm^3, respectively. In the control group, TV, iTV, aTV, and CRR were 2.27±0.21cm^3, 23.07±2.56cm^3, 36.14±3.72cm^3, and 1.73±0.15cm^3, respectively. aTV and CRR in the tumor group were significantly lower than those in the control group, with statistical differences (P<0.05). Excessive resection would lead to local collapse and deformation of the mammary gland, which would significantly change the appearance of the mammary gland after surgery (20). In the case of a negative margin, the less the amount of tissue removed, the higher the success rate of surgery was (21).

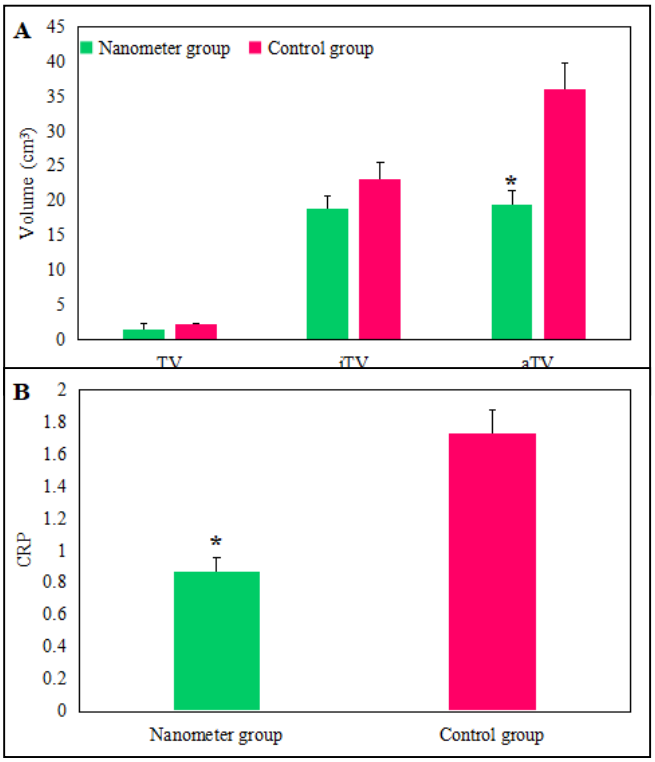

Figure 9. Comparison of TV between the two groups. (Figure A: Histogram of comparison of TV, iTV, and aTV between the two groups. Figure B: CRP histogram of the two groups.). (* represented statistical differences compared with the control group, P<0.05.)

Comparison of a surgical margin between the two groups

The positive rate of tumor margin (PR), the longest margin (Le), the shortest margin (Se), the differences between Le and the ideal margin (Dli), and the differences between Se and the ideal margin (Dsi) were compared between the two groups (Figure 10). PR of primary margin was 6.52% and 23.91% in the nano group and the control group, respectively. PR of

primary margin in the nano group was significantly lower than that in the control group (P<0.05). Le, Se, Dli, and Dsi values were 1.25±0.14cm, 0.58±0.06cm, 0.39±0.03cm, and 0.35±0.06cm, respectively. Le, Se, Dli, and Dsi values of the control group were 2.03 ± 0.18cm, 0.40 ± 0.03cm, 1.12 ± 0.17cm, and 0.71 ± 0.03cm, respectively. Le value in the tumor group was significantly lower than that in the control group (P<0.05), Se value was significantly higher than that in the control group (P<0.05). Dli and Dsi values in the tumor group were significantly lower than those in the control group (P<0.01). Margin status was an important influencing factor for postoperative local recurrence and the optimal PR of margin had an important influence on margin status (22-25).

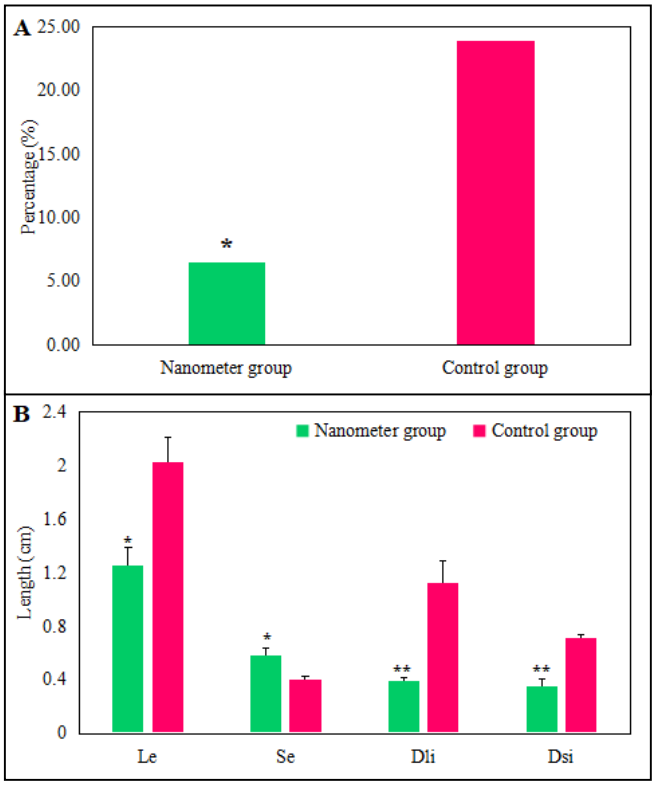

Figure 10. Comparison of surgical margins between the two groups. (Figure A: Histogram of PR between the two groups. Figure B: Histogram of Le, Se, Dli, and Dsi comparison between the two groups.). (* indicated significant differences compared with the control group, P<0.01. * represented statistical differences compared with the control group, P<0.05.).

Further statistical analysis was conducted on the distribution of Le and Se in the two groups (Figure 11). Compared with the control group, Le and Se in the tumor group were closer to Dli.

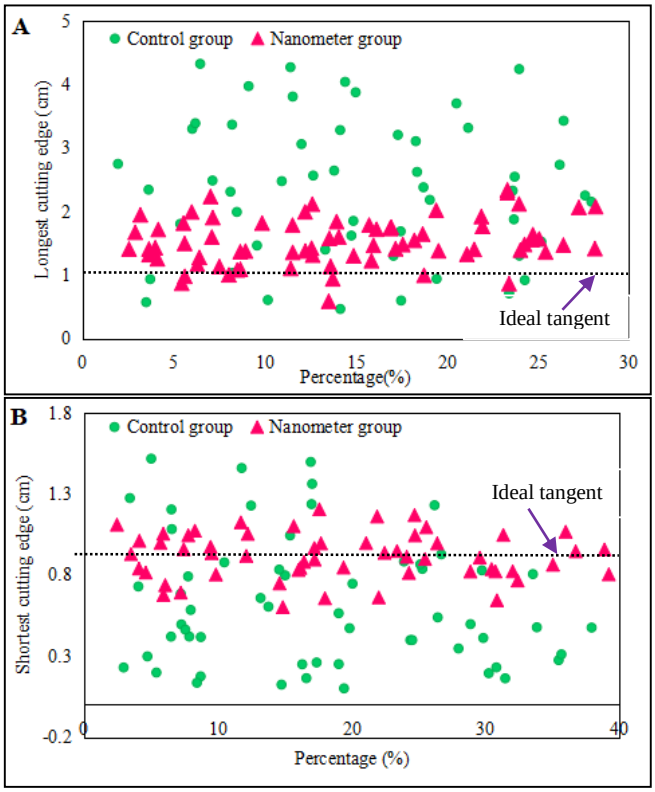

Figure 11. Comparison of the distribution of Le and Se between the two groups. (Figure A: Arrangement of the longest incision in the two groups. Figure B: Predestination diagram of the shortest cut in the two groups.)

Conclusions

In this study, MLU-MBs were prepared on account of Fe_3O_4 nanoparticles by PEI modification and the value of MLU-MBs in ultrasound localization-guided breast-conserving surgery for tumor resection was discussed. The results showed that MLU-MBs prepared in this study had a good image enhancement effect and could significantly reduce the PR of normal tissue resection and resection margin. However, there were still some shortcomings in this study. The differences between MLU-MBs as contrast agents in ultrasound imaging were only compared in this study. In future work, it will be further analyzed with other positioning methods to clarify its clinical value. In conclusion, MLU-MBs prepared in this study can improve the accuracy of ultrasound localization-guided breast-conserving surgery for tumor resection, which will provide a reference basis for the diagnosis and treatment of breast cancer.

Acknowledgments

Not applicable.

Interest conflict

The authors declare that they have no conflict of interest.

References

1. Tong M, Guo W. Indocyanine green fluorescence-guided lumpectomy of nonpalpable breast cancer versus wire-guided excision: A randomized clinical trial. Breast J. 2019 Mar;25(2):278-281. doi: 10.1111/tbj.13207. Epub 2019 Feb 22. PMID: 30801900.
2. Tong M, Guo W. Indocyanine green fluorescence-guided lumpectomy of nonpalpable breast cancer versus wire-guided excision: A randomized clinical trial. Breast J. 2019 Mar;25(2):278-281. doi: 10.1111/tbj.13207. Epub 2019 Feb 22. PMID: 30801900.
3. Weber WP, Soysal SD, Fulco I, Barandun M, Babst D, Kalbermatten D, Schaefer DJ, Oertli D, Kappos EA, Haug M. Standardization of oncoplastic breast conserving surgery. Eur J Surg Oncol. 2017 Jul;43(7):1236-1243. doi: 10.1016/j.ejso.2017.01.006. Epub 2017 Jan 31. PMID: 28214053.
4. Bertozzi N, Pesce M, Santi PL, Raposio E. Oncoplastic breast surgery: comprehensive review. Eur Rev Med Pharmacol Sci. 2017 Jun;21(11):2572-2585. PMID: 28678328.
5. Weber WP, Soysal SD, Fulco I, Barandun M, Babst D, Kalbermatten D, Schaefer DJ, Oertli D, Kappos EA, Haug M. Standardization of oncoplastic breast conserving surgery. Eur J Surg Oncol. 2017 Jul;43(7):1236-1243. doi: 10.1016/j.ejso.2017.01.006. Epub 2017 Jan 31. PMID: 28214053.
6. Sun Y, Liao M, He L, Zhu C. Comparison of breast-conserving surgery with mastectomy in locally advanced breast cancer after good response to neoadjuvant chemotherapy: A PRISMA-compliant systematic review and meta-analysis. Medicine (Baltimore). 2017 Oct;96(43):e8367. doi: 10.1097/MD.0000000000008367. PMID: 29069026; PMCID: PMC5671859.
7. Moo TA, Sanford R, Dang C, Morrow M. Overview of Breast Cancer Therapy. PET Clin. 2018 Jul;13(3):339-354. doi: 10.1016/j.cpet.2018.02.006. PMID: 30100074; PMCID: PMC6092031.
8. Sinnadurai S, Kwong A, Hartman M, Tan EY, Bhoo-Pathy NT, Dahlui M, See MH, Yip CH, Taib NA, Bhoo-Pathy N. Breast-conserving surgery versus mastectomy in young women with breast cancer in Asian settings. BJS Open. 2018 Oct 18;3(1):48-55. doi: 10.1002/bjs5.50111. PMID: 30734015; PMCID: PMC6354186.
9. Versluis M, Stride E, Lajoinie G, Dollet B, Segers T. Ultrasound Contrast Agent Modeling: A Review. Ultrasound Med Biol. 2020 Sep;46(9):2117-2144. doi: 10.1016/j.ultrasmedbio.2020.04.014. Epub 2020 Jun 13. PMID: 32546411.
10. Turco S, Frinking P, Wildeboer R, Arditi M, Wijkstra H, Lindner JR, Mischi M. Contrast-Enhanced Ultrasound Quantification: From Kinetic Modeling to Machine Learning. Ultrasound Med Biol. 2020 Mar;46(3):518-543. doi: 10.1016/j.ultrasmedbio.2019.11.008. Epub 2020 Jan 8. PMID: 31924424.
11. Borden MA, Song KH. Reverse engineering the ultrasound contrast agent. Adv Colloid Interface Sci. 2018 Dec;262:39-49. doi: 10.1016/j.cis.2018.10.004. Epub 2018 Oct 24. PMID: 30396507; PMCID: PMC6268001.
12. Ebelt H, Offhaus A, Wiora M, Roehl P, Schwenzky A, Weida A, Hoyme M, Bindemann-Koecher J, Anacker J. Impact of ultrasound contrast agent on the detection of thrombi during transoesophageal echocardiography. Open Heart. 2019 Sep 26;6(2):e001024. doi: 10.1136/openhrt-2019-001024. PMID: 31673382; PMCID: PMC6803001.
13. Yang F, Chun LF, Chen ZY. Inducing Tumor Cell Apoptosis: Mediated Survivin miRNA by Ultrasound and Cationic Lipid Contrast Agent. Curr Mol Med. 2020 Sep 9. doi: 10.2174/1566524020666200909164513. Epub ahead of print. PMID: 32912126.
14. Lau C, Rivas M, Dinalo J, King K, Duddalwar V. Scoping Review of Targeted Ultrasound Contrast Agents in the Detection of Angiogenesis. J Ultrasound Med. 2020 Jan;39(1):19-28. doi: 10.1002/jum.15072. Epub 2019 Jun 24. PMID: 31237009.
15. Du M, Chen Y, Tu J, Liufu C, Yu J, Yuan Z, Gong X, Chen Z. Ultrasound Responsive Magnetic Mesoporous Silica Nanoparticle-Loaded Microbubbles for Efficient Gene Delivery. ACS Biomater Sci Eng. 2020 May 11;6(5):2904-2912. doi: 10.1021/acsbiomaterials.0c00014. Epub 2020 Apr 13. PMID: 33463299.
16. Yan L, Miao W, Li D. Ultrasound Imaging Based on Magnetic Lipid Microbubble Contrast Agent with Fe_3O_4 Nanoparticles. J Nanosci Nanotechnol. 2020 Oct 1;20(10):6087-6093. doi: 10.1166/jnn.2020.18519. PMID: 32384956.
17. Dong W , Huang A , Huang J , Wu P , Guo S , Liu H , Qin M , Yang X , Zhang B , Wan M , Zong Y. Plasmid-loadable magnetic/ultrasound-responsive nanodroplets with a SPIO-NP dispersed perfluoropentane core and lipid shell for tumor-targeted intracellular plasmid delivery. Biomater Sci. 2020 Oct 7;8(19):5329-5345. doi: 10.1039/d0bm00699h. Epub 2020 Aug 14. PMID: 32793943.
18. Beguin E, Bau L, Shrivastava S, Stride E. Comparing Strategies for Magnetic Functionalization of Microbubbles. ACS Appl Mater Interfaces. 2019 Jan 16;11(2):1829-1840. doi: 10.1021/acsami.8b18418. Epub 2019 Jan 7. PMID: 30574777.
19. Feshitan JA, Vlachos F, Sirsi SR, Konofagou EE, Borden MA. Theranostic Gd(III)-lipid microbubbles for MRI-guided focused ultrasound surgery. Biomaterials. 2012 Jan;33(1):247-55. doi:

10.1016/j.biomaterials.2011.09.026. Epub 2011 Oct 10. PMID: 21993236; PMCID: PMC4030396.

20. Volders JH, Negenborn VL, Spronk PE, Krekel NMA, Schoonmade LJ, Meijer S, Rubio IT, van den Tol MP. Breast-conserving surgery following neoadjuvant therapy-a systematic review on surgical outcomes. Breast Cancer Res Treat. 2018 Feb;168(1):1-12. doi: 10.1007/s10549-017-4598-5. Epub 2017 Dec 6. Erratum in: Breast Cancer Res Treat. 2018 Jan 11;: PMID: 29214416; PMCID: PMC5847047.
21. Omranipour R. Surgery for Pregnancy-Associated Breast Cancer. Adv Exp Med Biol. 2020;1252:95-99. doi: 10.1007/978-3-030-41596-9_12. PMID: 32816267.
22. Dodaro CA, Zaffiro A, Iannicelli AM, Giordano L, Sorbino L, Mangiapia F, Lanzano M, Schonauer F. Combined Timed Surgery and Conservative Management of Primary Necrotizing Fasciitis of the Breast: A Case Report. Am J Case Rep. 2020 Jun 3;21:e922688. doi: 10.12659/AJCR.922688. PMID: 32487979; PMCID: PMC7295313.
23. Moradi S, Khaledian S, Abdoli M, Shahlaei M, Kahrizi D. Nano-biosensors in cellular and molecular biology. Cell Mol Biol 2018;64(5):85-90. doi:10.14715/cmb/2018.64.5.14.
24. Olfati A, Kahrizi D, Balaky ST, Sharifi R, Tahir MB, Darvishi E. Green synthesis of nanoparticles using Calendula officinalis extract from silver sulfate and their antibacterial effects on Pectobacterium caratovorum. Inorg Chem Commun 2021;125:108439. doi: 10.1016/j.inoche.2020.108439.
25. Khaledian S, Kahrizi D, Balaky ST, Arkan E, Abdoli M, Martinez F. Electrospun nanofiber patch based on gum tragacanth/polyvinyl alcohol/molybdenum disulfide composite for tetracycline delivery and their inhibitory effect on Gram+ and Gram–bacteria. J Mol Liq 2021 Jul 15;334:115989. doi: 10.1016/j.molliq.2021.115989.